The Plant Cell, Vol. 26: 2129–2142, May 2014, www.plantcell.org

SAUR Inhibition of PP2C-D Phosphatases Activates Plasma Membrane H+-ATPases to Promote Cell Expansion in *Arabidopsis*[C][W]

Angela K. Spartz,[a,1] Hong Ren,[a,1] Mee Yeon Park,[a] Kristin N. Grandt,[a] Sang Ho Lee,[a,2] Angus S. Murphy,[b] Michael R. Sussman,[c] Paul J. Overvoorde,[d] and William M. Gray[a,3]

[a] Department of Plant Biology, University of Minnesota, St. Paul, Minnesota 55108
[b] Department of Plant Science and Landscape Architecture, University of Maryland, College Park, Maryland 20742
[c] Biotechnology Center and Department of Biochemistry, University of Wisconsin, Madison, Wisconsin 53706
[d] Department of Biology, Macalester College, St. Paul, Minnesota 55105

The plant hormone auxin promotes cell expansion. Forty years ago, the acid growth theory was proposed, whereby auxin promotes proton efflux to acidify the apoplast and facilitate the uptake of solutes and water to drive plant cell expansion. However, the underlying molecular and genetic bases of this process remain unclear. We have previously shown that the *SAUR19-24* subfamily of auxin-induced *SMALL AUXIN UP-RNA* (*SAUR*) genes promotes cell expansion. Here, we demonstrate that SAUR proteins provide a mechanistic link between auxin and plasma membrane H+-ATPases (PM H+-ATPases) in *Arabidopsis thaliana*. Plants overexpressing stabilized SAUR19 fusion proteins exhibit increased PM H+-ATPase activity, and the increased growth phenotypes conferred by SAUR19 overexpression are dependent upon normal PM H+-ATPase function. We find that SAUR19 stimulates PM H+-ATPase activity by promoting phosphorylation of the C-terminal autoinhibitory domain. Additionally, we identify a regulatory mechanism by which SAUR19 modulates PM H+-ATPase phosphorylation status. SAUR19 as well as additional SAUR proteins interact with the PP2C-D subfamily of type 2C protein phosphatases. We demonstrate that these phosphatases are inhibited upon SAUR binding, act antagonistically to SAURs in vivo, can physically interact with PM H+-ATPases, and negatively regulate PM H+-ATPase activity. Our findings provide a molecular framework for elucidating auxin-mediated control of plant cell expansion.

INTRODUCTION

The phytohormone auxin regulates plant growth and development by controlling the fundamental processes of cell division, expansion, and differentiation. While substantial progress has been made regarding the signaling mechanisms underlying auxin-regulated gene expression (Chapman and Estelle, 2009), the mechanisms by which these changes in expression direct specific physiological and developmental outputs are less clear.

SMALL AUXIN UP-RNA (*SAUR*) genes comprise the largest family of auxin-induced genes, with 79 members in *Arabidopsis thaliana* (Hagen and Guilfoyle, 2002). Recent studies of the *SAUR19* and *SAUR63* subfamilies have implicated these SAURs as positive effectors of cell expansion (Franklin et al., 2011; Chae et al., 2012; Spartz et al., 2012). SAUR19 family proteins are highly unstable. However, the addition of an N-terminal green fluorescent protein (GFP) or StrepII epitope tag increases SAUR19 stability and confers numerous phenotypes indicative of increased and/or unregulated cell expansion, including increased hypocotyl and leaf size, altered tropic responses, and defects in apical hook maintenance (Spartz et al., 2012). Likewise, SAUR63 fusion proteins confer several cell expansion phenotypes, including increases in hypocotyl, petal, and stamen length (Chae et al., 2012).

These findings, together with the observation that these SAUR proteins associate with the plasma membrane (Chae et al., 2012; Spartz et al., 2012), prompted us to examine the possibility that SAURs promote cell expansion by regulating plasma membrane (PM) H+-ATPases. PM H+-ATPases have long been hypothesized to promote auxin-mediated cell expansion via an acid growth mechanism (Rayle and Cleland, 1970; Rayle and Cleland, 1980, 1992; Hager, 2003). In this model, auxin activates PM H+-ATPases to lower apoplastic pH, thereby activating expansins and other cell wall–modifying proteins. The increase in PM H+-ATPase activity also results in plasma membrane hyperpolarization, leading to solute uptake, which in turn promotes water uptake to provide the turgor pressure to drive cell expansion. *Arabidopsis* contains 11 genes encoding PM H+-ATPases (*AHA1-11*; Baxter et al., 2003). By far, *AHA1* and *AHA2* encode the two most highly expressed isoforms (Baxter et al., 2003; Haruta et al., 2010). Recent molecular evidence provides important support for the acid growth model, as auxin was found to rapidly activate *Arabidopsis* PM

[1] These authors contributed equally to this work.
[2] Current address: College of Techno-Sciences, Mokwon University, 88 Doanbuk-ro, Daejeon, 302-729, South Korea.
[3] Address correspondence to grayx051@umn.edu.
The author responsible for distribution of materials integral to the findings presented in this article in accordance with the policy described in the Instructions for Authors (www.plantcell.org) is: William M. Gray (grayx051@umn.edu).
[C] Some figures in this article are displayed in color online but in black and white in the print edition.
[W] Online version contains Web-only data.
www.plantcell.org/cgi/doi/10.1105/tpc.114.126037

H^+-ATPases by promoting phosphorylation of the penultimate threonine residue (corresponding to Thr-947 of AHA2) within the C-terminal autoinhibitory domain (Takahashi et al., 2012). Phosphorylation of this residue coincides with 14-3-3 protein binding and activation of the pump (Fuglsang et al., 1999; Kinoshita and Shimazaki, 1999; Jelich-Ottmann et al., 2001). Additionally, tobacco (*Nicotiana tabacum*) plants engineered to express a constitutively active PM H^+-ATPase derivative lacking the C-terminal inhibitory domain exhibit several phenotypes indicative of increased cell expansion (Gévaudant et al., 2007). In contrast to the effects of auxin, Hayashi et al. (2014) recently reported that abscisic acid–mediated inhibition of hypocotyl elongation correlates with a reduction in Thr-947 phosphorylation. Together, these findings strongly indicate that the C-terminal autoinhibitory domain of PM H^+-ATPases plays an important role in controlling plant cell expansion.

A major gap in the acid growth model is the mechanism by which auxin actually promotes H^+-ATPase phosphorylation or otherwise activates the pump. In part, auxin may increase PM H^+-ATPase activity by regulating gene expression, as auxin promotes expression of at least one major PM H^+-ATPase isoform in maize (*Zea mays*; Frías et al., 1996). However, auxin-mediated activation of PM H^+-ATPase gene expression has not been demonstrated in *Arabidopsis* or other dicots. A second possible mechanism of auxin action is the inhibition of PM H^+-ATPase endocytosis (Paciorek et al., 2005; Robert et al., 2010). In this study, we elucidate a mechanism by which auxin-induced *SAUR* genes activate PM H^+-ATPases by promoting Thr-947 phosphorylation. We demonstrate that SAUR proteins inhibit the activity of a family of type 2C protein phosphatases (PP2Cs), which in turn modulate PM H^+-ATPase phosphorylation status to regulate cell expansion.

RESULTS

SAUR19 Overexpression Confers Increased PM H^+-ATPase Activity

To examine whether SAUR proteins might play a role in PM H^+-ATPase activation, we compared plants overexpressing stabilized SAUR19 fusion proteins (35S:GFP-SAUR19 and 35S:StrepII-SAUR19; Spartz et al., 2012) to *OPEN STOMATA2* (*ost2-2*) plants, which contain a constitutively active allele of the PM H^+-ATPase encoded by *AHA1* (Merlot et al., 2007). The membrane hyperpolarization conferred by *ost2-2* prevents stomatal closure, resulting in drought hypersensitivity. *ost2* mutants also constitutively express pathogen defense genes (Merlot et al., 2007). Similar phenotypes are elicited by fusicoccin (FC), a fungal wilting toxin that binds to and activates PM H^+-ATPases (Marre, 1979; Singh and Roberts, 2004). Plants overexpressing GFP- or StrepII-SAUR19 fusion proteins displayed all of these phenotypes. Expression of *PATHOGENESIS RELATED PROTEIN1* and the *DEFENSIN PDF1.2* were significantly upregulated in GFP-SAUR19 seedlings (Figure 1A). Likewise, *SAUR19*-overexpressing plants displayed enhanced water loss in leaf detachment assays (Figure 1B), wilted faster than wild-type controls upon cessation of watering, and exhibited delayed stomatal closure (Supplemental Figures 1A and 1B). Also, like *ost2* mutants and consistent with increased proton pump activity, overexpression of SAUR19 fusion proteins resulted in increased media acidification (Figure 1C). As these findings suggested that the increased cell expansion phenotypes of SAUR19 overexpression plants may be the result of elevated PM H^+-ATPase activity, we measured the apoplastic pH of rosette leaves. Consistent with this possibility, apoplastic pH was significantly diminished in both GFP-SAUR19 and StrepII-SAUR19 leaves (Figure 1D). Lastly, we found that like these *SAUR19* transgenic lines, *ost2* seedlings exhibited previously undescribed increases in hypocotyl length, cotyledon size, and reduced apical hook maintenance compared with wild-type controls (Supplemental Figures 1C and 1D). Thus, SAUR19 gain-of-function plants exhibit remarkable phenotypic similarity to the constitutively active *ost2-2* PM H^+-ATPase mutant.

We conducted similar comparisons to loss-of-function PM H^+-ATPase mutants. *AHA1* and *AHA2* encode the two most abundant PM H^+-ATPase isoforms (Haruta et al., 2010). While *aha1 aha2* double mutants display embryo lethality, single mutants exhibit modest phenotypes consistent with a reduced proton motive force, including impaired root growth on alkaline pH and mild resistance to alkali metals, other toxic cations, and aminoglucoside antibiotics (Haruta et al., 2010; Haruta and Sussman, 2012). In contrast, SAUR19 overexpression plants exhibit opposite phenotypes in these assays. For example, SAUR19 overexpression conferred hypersensitivity to LiCl, arginine, and gentamicin (Figures 1E; Supplemental Figures 1E and 1F). Of these compounds, LiCl had the most dramatic effect, not only inhibiting root growth of SAUR19 transgenic seedlings to a much greater extent than the wild type, but also causing increased leaf chlorosis. To determine if SAUR19 overexpression phenotypes require normal H^+ pump function, we crossed the StrepII-SAUR19 transgene into the *aha2-4* mutant background. The long hypocotyl, LiCl hypersensitivity, and several additional phenotypes conferred by StrepII-SAUR19 were significantly attenuated by the *aha2-4* mutation (Figures 1F and 1G), demonstrating that the phenotypes conferred by SAUR19 overexpression require PM H^+-ATPases.

The above findings suggest that SAUR19 activates PM H^+-ATPases. PM H^+-ATPase activation requires phosphorylation of the penultimate amino acid (Thr-947 in AHA2) of the C-terminal autoinhibitory domain and subsequent binding of a 14-3-3 protein to this phosphosite (Fuglsang et al., 1999). Recently, auxin treatment of hypocotyl segments was found to increase Thr-947 phosphorylation and 14-3-3 binding (Takahashi et al., 2012). We examined Thr-947 phosphorylation status in SAUR19 overexpression lines utilizing a GST-14-3-3 far-western gel blotting assay that has been widely used to assess H^+ pump activation (Fuglsang et al., 1999; Kinoshita and Shimazaki, 2001; Hayashi et al., 2010). To validate the efficacy of this assay in our hands, we first examined GST-14-3-3 binding to blots containing plasma membrane fractions prepared from mock- or FC-treated wild-type seedlings, as well as plasma membrane fractions subjected to an in vitro dephosphorylation treatment (Hayashi et al., 2010). A single predominant α-GST reactive band was detected at the predicted 105 kD mass of AHA proteins (Figure 1H, left). As previously reported (Hayashi et al.,

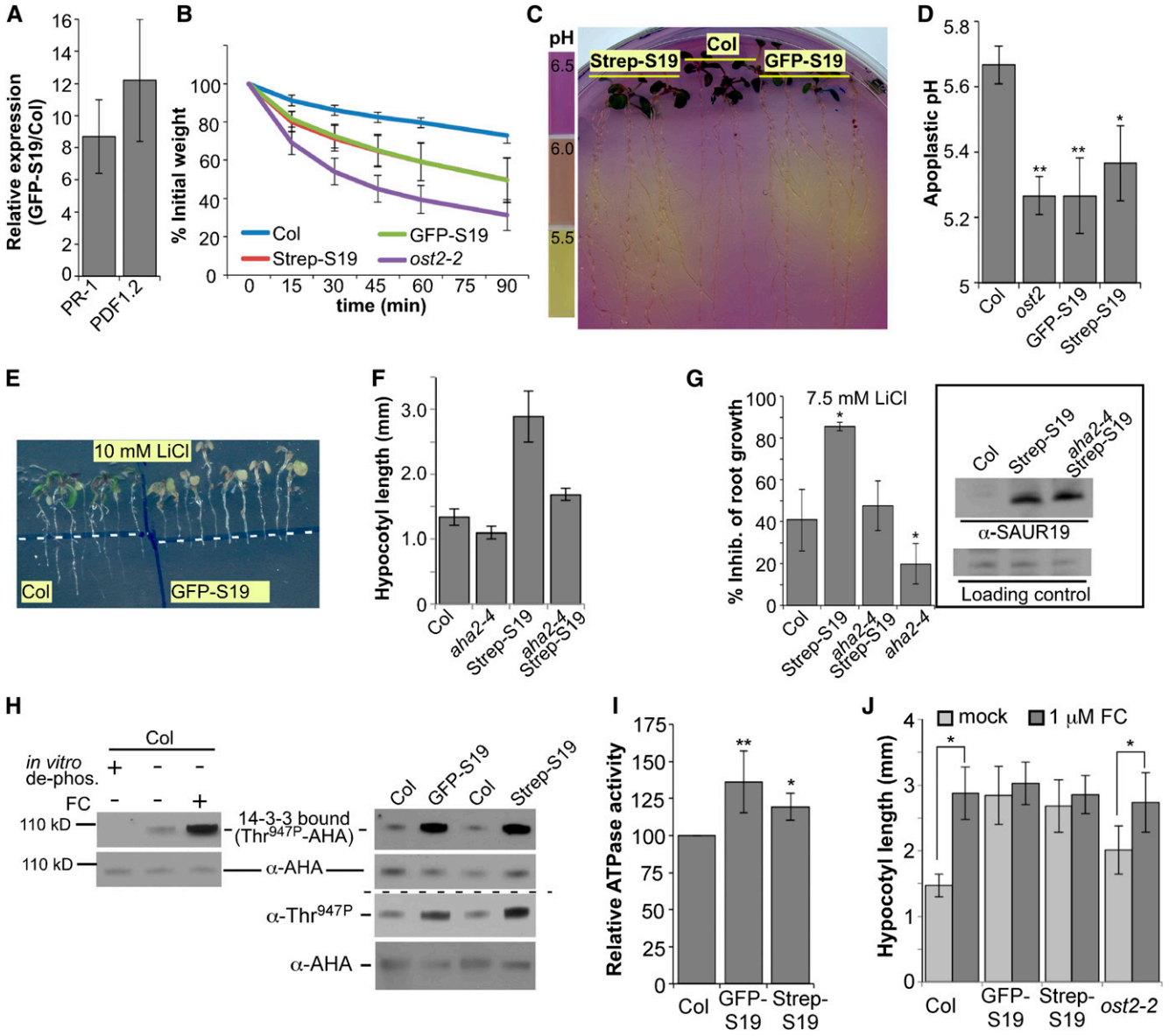

Figure 1. SAUR19 Activates PM H+-ATPases.

(A) Quantitative RT-PCR analysis of *PR-1* and *PDF1.2* expression in 7-d-old Col and GFP-SAUR19 (GFP-S19) seedlings. Error bars depict SD obtained from three biological replicates.

(B) Kinetics of water loss in leaf detachment assays. Data points depict mean weights of 10 leaves/genotype ± SD. All genotypes exhibit significant differences from Col at all time points ($P \leq 0.05$).

(C) Twelve-day-old seedlings were transferred to plates containing the pH indicator dye bromocreol purple. Color changes were recorded after 8 h.

(D) Leaf apoplastic pH; mean ($n = 3$) ± SD. Asterisks indicate significant difference from Col control by one-way ANOVA (**$P < 0.01$; *$P < 0.05$).

(E) Col and GFP-SAUR19 seedlings were transferred to media containing 10 mM LiCl and grown for 4 d. White lines indicate root tip position at the time of transfer.

(F) and **(G)** *aha2-4* partially suppresses the long hypocotyl **(F)** and LiCl hypersensitivity **(G)** phenotypes of StrepII-SAUR19 seedlings. Values represent sample means ± SD ($n \geq 15$). Inset: α-SAUR19 immunoblot confirming equivalent levels of StrepII-SAUR19 protein. For **(F)**, all means are significantly different ($P < 0.01$) from one another by one-way ANOVA. For **(G)**, asterisk indicates significant difference ($P < 0.01$) from Col control.

(H) Right: Increased C-terminal phosphorylation of PM H+-ATPases in GFP-SAUR19 and StrepII-SAUR19 seedlings. Levels of Thr-947-phosphorylated AHA proteins as monitored by GST-14-3-3 binding or α-Thr947P immunoblotting. Separate blots were used for the two experiments. Left: Plasma membranes prepared from untreated or FC treated (30 min) seedlings. Sample in the first lane was subjected to in vitro dephosphorylation (Hayashi et al., 2010).

(I) Relative vanadate-sensitive ATP hydrolytic activity in plasma membrane fractions prepared from 6-d-old etiolated seedlings. Values represent the means ± SD obtained from three biological replicates. Asterisks indicates significant difference from Col as determined by one-way ANOVA (**$P < 0.01$; *$P < 0.05$).

(J) FC promotes hypocotyl elongation of Col but not SAUR19 overexpressing seedlings. Three-day-old seedlings were transferred to media containing 1 μM FC and grown an additional 3 d. Asterisks indicate significant effect of FC as determined by one-way ANOVA ($P < 0.01$).

2010), in vitro dephosphorylation abolished and FC treatment increased GST-14-3-3 binding, confirming that this assay is an effective proxy for assessing Thr-947 phosphorylation status. When compared with wild-type controls, a clear increase in Thr-947 phosphorylation, but not total AHA protein abundance, was apparent in both the GFP- and StrepII-SAUR19 samples (Figure 1H, right). To further confirm the validity of the phosphorylation increase observed in the SAUR19 samples by far-western assays, we obtained the previously described Thr-947 phospho-specific antibody (Hayashi et al., 2010). Immunoblot analysis with the α-Thr^{947P} antibody also detected increased C-terminal phosphorylation of PM H$^+$-ATPases in both GFP- and StrepII-SAUR19 membranes (Figure 1H). To test whether this increase in phosphorylation might be an indirect consequence of constitutive SAUR19 overexpression, we repeated this assay using seedlings expressing an inducible GFP-SAUR19 transgene. Increased 14-3-3 binding was apparent with inductions as short as 4 h (Supplemental Figure 1G).

To directly assess PM H$^+$-ATPase activity, we measured the vanadate-sensitive ATP hydrolytic activity present in plasma membrane fractions prepared from Columbia (Col), GFP-SAUR19, and StrepII-SAUR19 seedlings. Compared with Col plasma membranes, membranes prepared from SAUR19 overexpression lines displayed a 20 to 35% increase in ATPase activity (Figure 1I).

The above findings demonstrate that PM H$^+$-ATPases are constitutively active in SAUR19 overexpression seedlings. We therefore hypothesized that unlike wild-type seedlings, the SAUR19 overexpression lines would not exhibit hypocotyl elongation in response to fusicoccin. Indeed, whereas 1 μM FC promoted greater than a 2-fold increase in Col hypocotyl growth, both GFP- and StrepII-SAUR19 seedlings were unaffected (Figure 1J). The *ost2-2* mutant also exhibited a diminished response to FC treatment. Similar findings were obtained when we examined indole-3-acetic acid (IAA) promotion of hypocotyl elongation (Supplemental Figure 1H).

SAUR Proteins Negatively Regulate PP2C-D Phosphatase Activity

Yeast two-hybrid screens with SAUR19 identified three members of the nine-member D-clade of PP2Cs (Figure 2A). A search of the *Arabidopsis* Interactome AI-1 database (Arabidopsis Interactome Mapping Consortium, 2011) identified four additional SAUR proteins (SAUR9, 38, 40, and 72) that also interact with D-clade PP2Cs (Supplemental Figure 2A). While little is known about the function of D-clade phosphatases, the expression of *PP2C-D1* is induced by auxin (Nemhauser et al., 2006). Additionally, most D-clade PP2Cs contain a predicted membrane spanning domain (Schweighofer et al., 2004).

To begin to characterize the PP2C-D1 protein, we raised antibodies against a recombinant 6xHis-PP2C-D1 fusion protein. Immunoblot analysis with this antibody detected a 45-kD band in wild-type extracts. This band was absent in extracts prepared from *pp2c-d1* mutant seedlings (SALK_099356) and increased in extracts prepared from seedlings expressing a Pro35S:*PP2C-D1* transgene (Supplemental Figure 2B). To investigate whether the PP2C-D1 protein is associated with the plasma membrane, we used this antibody to analyze fractionated extracts by immunoblotting. Like PM H$^+$-ATPases and SAUR19, strong enrichment of the PP2C-D1 signal was observed in the plasma membrane–enriched fraction (Figure 2B). In contrast, the endoplasmic reticulum–associated protein SEC12 was highly enriched in the "other membrane" fraction.

To further validate the SAUR19/PP2C-D1 two-hybrid interaction, we conducted coimmunoprecipitation assays using solubilized microsomal extracts prepared from either GFP-SAUR19 or GFP-SAUR19[35S:PP2C-D1] seedlings. GFP-SAUR19 was observed in α-PP2C-D1 precipitates but not in control reactions using the preimmune sera (Figure 2C). Introduction of a 35S:PP2C-D1 transgene resulted in a strong increase in both PP2C-D1 levels and the amount of GFP-SAUR19 that coimmunoprecipitated, suggesting that PP2C-D1 abundance may be limiting.

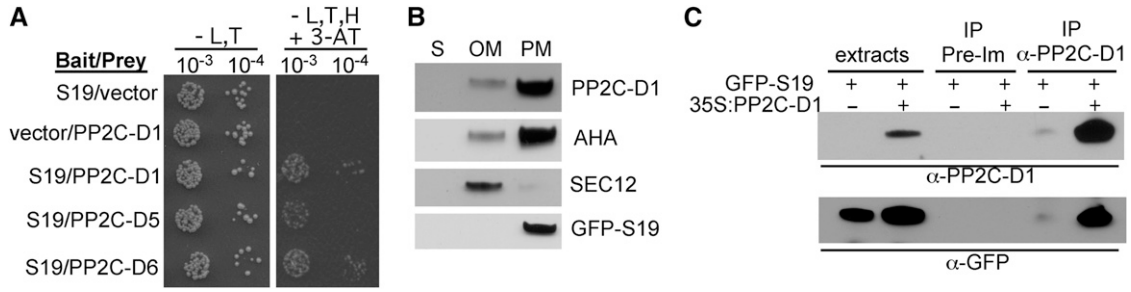

Figure 2. SAUR19 Interacts with D-Clade PP2Cs.

(A) Yeast two-hybrid interaction between SAUR19 and three D-clade PP2Cs. Serial dilutions of yeast cells harboring a P_{GAL}:*HIS3* reporter were spotted onto selective media lacking histidine and supplemented with 10 mM 3-aminotriazole.

(B) Immunoblot analysis of soluble (S), lower phase-enriched other membrane (OM), and upper phase-enriched PM fractions from 7-d-old GFP-SAUR19[35S:PP2C-D1] seedlings. Five micrograms of each fraction were loaded onto the gel.

(C) Coimmunoprecipitation of GFP-SAUR19 and PP2C-D1 from 7-d-old seedlings. PP2C-D1 was immunoprecipitated from solubilized microsomal extracts prepared from GFP-SAUR19 or GFP-SAUR19[35S:PP2C-D1] seedlings. Precipitates were then immunoblotted with α-PP2C-D1 (top) and α-GFP (bottom) antibodies. The middle two lanes show control immunoprecipitations using preimmune sera.

We next examined the possibility that SAUR19 binding regulates PP2C-D1 activity. In in vitro phosphatase assays employing the chromogenic substrate *p*-nitrophenylphosphate (pNPP), recombinant PP2C-D1 exhibited phosphatase activity. This activity was reduced by the addition of GST-SAUR19, but not GST alone (Figure 3A). SAUR19 inhibition of PP2C-D1 occurred independent of substrate concentration (Figure 3B). While the K_m was unaffected by the addition of GST-SAUR19, a 2-fold reduction in V_{max} was observed, consistent with a non-competitive mode of inhibition (Figure 3C). GST-SAUR19 inhibition of PP2C-D1 activity saturated at ~50% (Supplemental Figure 2C). Given that *Arabidopsis* encodes 79 SAUR proteins and nine D-clade PP2Cs, we examined the possibility that other SAUR/PP2C-D combinations might display stronger inhibition. Indeed, SAUR9 inhibited PP2C-D1 to a much greater extent than SAUR19, with SAUR40 and SAUR72 exhibiting comparable inhibition. Additionally, other PP2C-D family members displayed distinct regulatory interactions with the different SAUR proteins tested (Figure 3D). While some level of inhibition was apparent for nearly all SAUR/PP2C-D combinations tested, none of the SAUR proteins affected phosphatase activity of the well-characterized A-clade PP2C, ABI1. Furthermore, activities of neither the E-clade PP2C At3g06270 nor the PPP-phosphatase PP7 were inhibited by SAUR9. The negative regulation of PP2C-D activity by SAUR binding is reminiscent of the PYR/PYL/RCAR family of abscisic acid (ABA) receptors and their inhibition of several A-clade PP2Cs (Ma et al., 2009; Park et al., 2009). However, whereas the ABA receptors require ligand binding to interact with PP2Cs, we observed no such effect of the addition of auxin to assays examining SAUR19/PP2C-D interactions (Supplemental Figure 2D online).

PP2C-D1 Negatively Regulates PM H+-ATPase Activity

Prior biochemical studies have suggested that Thr-947 of PM H+-ATPases is dephosphorylated by a plasma membrane–associated Mg^{2+}/Mn^{2+}-dependent phosphatase (Hayashi et al., 2010). PP2Cs are distinguished from other phosphatases by their requirement for divalent cations (Cohen, 1989). We therefore tested the ability of PP2C-D1 to regulate the PM H+-ATPase encoded by *AHA2* by expressing these proteins in yeast. In strain RS-72, the endogenous yeast H^+ pump, *PMA1*, is under control of the *GAL1* promoter; therefore, cells are only viable when grown on galactose media (Fuglsang et al., 1999, 2007). When *AHA2* is expressed in this strain, Thr-947 is phosphorylated by an endogenous kinase, enabling *AHA2* to complement P_{GAL1}*:PMA1* and restore growth on glucose media (Fuglsang et al., 1999). However, when we coexpressed *PP2C-D1* with *AHA2*, RS-72 was again unable to grow on glucose, demonstrating that PP2C-D1 negatively regulates AHA2 function

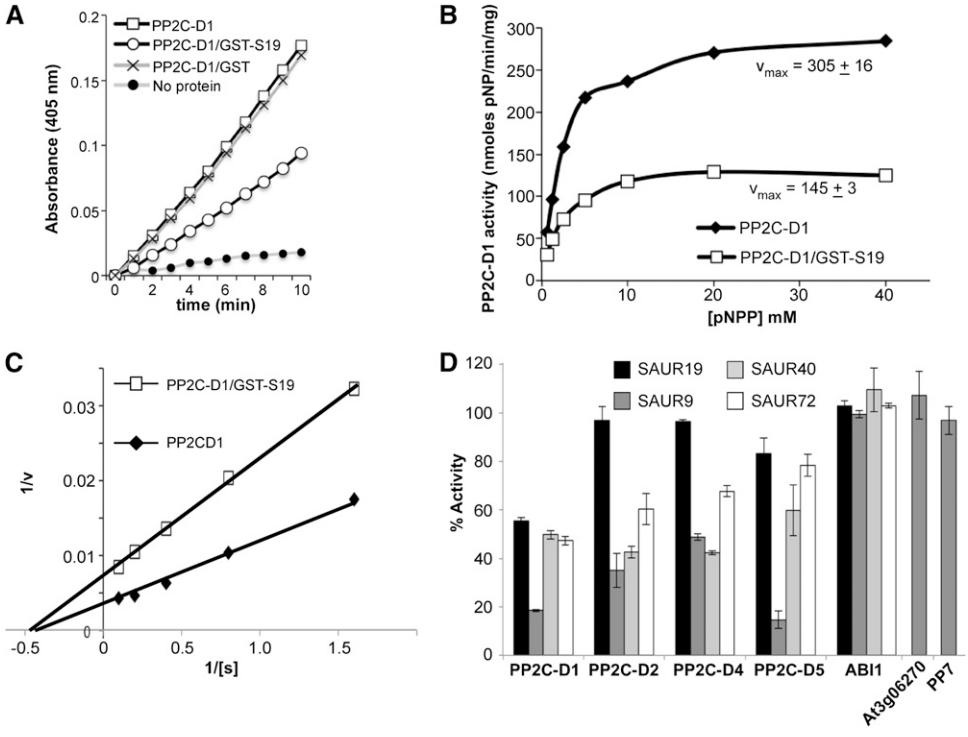

Figure 3. SAUR Proteins Inhibit PP2C-D Enzyme Activity.

(A) pNPP phosphatase assays containing 0.2 μM GST-PP2C-D1 ± 1 μM GST or GST-SAUR19.

(B) Substrate dependence of PP2C-D1 in the presence or absence of a 4-fold molar excess of GST-SAUR19.

(C) Lineweaver-Burk plot of the 0 to 10 mM data shown in **(B)**.

(D) Phosphatase activities of various PP2Cs in the presence of an 8-fold molar excess of different 6xHis-SAUR proteins. Values represent the mean (n = 3) ± SD.

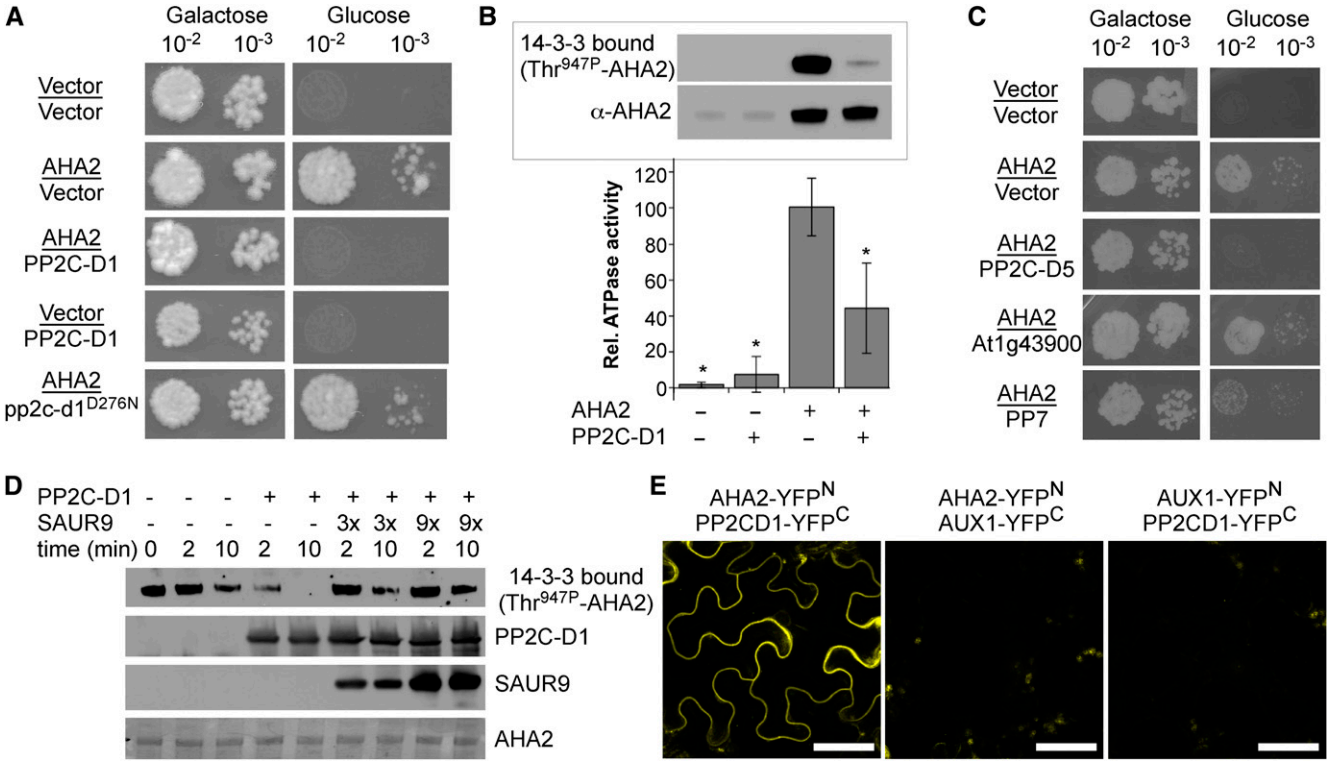

Figure 4. PP2C-D1 Functional and Physical Interactions with AHA2.

(A) Expression of *PP2C-D1* in yeast abolishes *AHA2* complementation of PM H^+-ATPase activity.

(B) Far-western gel blot analysis of Thr-947 phosphorylation (top) and relative ATPase activity (bottom) of yeast plasma membranes prepared from cells expressing AHA2 alone or AHA2 and PP2C-D1. Activity shown is the vanadate-sensitive fraction. Data shown is the mean of three biological replicates ± SD. Asterisks indicate significant difference from the AHA2 sample ($P < 0.01$).

(C) PP2C-D5, but not the At1g43900 or PP7 phosphatases, also inhibits AHA2 in yeast.

(D) In vitro phosphatase assay examining PP2C-D1 dephosphorylation of yeast-expressed AHA2. Where indicated, 6xHis-SAUR9 was added to a 3- or 9-fold molar excess relative to PP2C-D1.

(E) Bimolecular fluorescence complementation assay with PP2C-D1 and AHA2. The indicated split YFP constructs were transiently coexpressed in tobacco leaves and fluorescent images of epidermal cells obtained by confocal microscopy. Bars = 50 μm.

[See online article for color version of this figure.]

(Figure 4A). To test whether PP2C-D1 phosphatase activity is required for this inhibition, we used site-directed mutagenesis to introduce a $D^{276}N$ mutation within the highly conserved metal binding domain (Das et al., 1996). In vitro phosphatase assays confirmed that this mutation abolished PP2C-D1 activity (Supplemental Figure 3A). When coexpressed with *AHA2* in RS-72 cells, the phosphatase-dead pp2c-$d1^{D276N}$ had no effect on the ability of AHA2 to support growth on glucose media, demonstrating that phosphatase activity is required for PP2C-D1 inhibition of AHA2 function (Figure 4A). α-PP2C-D1 immunoblot analysis of yeast extracts confirmed that the wild-type and $D^{276}N$ derivative were expressed at similar levels (Supplemental Figure 3B). We also attempted to reconstitute the entire AHA2/PP2C-D1/SAUR regulatory circuit in yeast. However, we observed very poor expression of both SAUR19 and SAUR9 in this heterologous system, which prevented us from testing the possibility that SAURs can reverse the effects of PP2C-D1 on AHA2 function in yeast.

To determine if PP2C-D1 negatively regulates AHA2 in yeast by dephosphorylating Thr-947, we isolated yeast plasma membranes and subjected them to both 14-3-3 far-western gel blot analysis and ATP hydrolysis assays. A striking reduction in Thr-947 phosphorylation was apparent in membranes prepared from cells coexpressing PP2C-D1 (Figure 4B). Furthermore, this reduction in Thr-947 phosphorylation correlated with a reduction in vanadate-sensitive ATPase activity. Together, these findings demonstrate that when expressed in yeast, PP2C-D1 negatively regulates AHA2 by dephosphorylating Thr-947.

To examine the specificity of PP2C-D1 inhibition of AHA2 activity in yeast, we constructed additional phosphatase expression clones that we coexpressed with AHA2 in RS-72. Like PP2C-D1, PP2C-D5 also inhibited AHA2 (Figure 4C). However, expression of either At1g43900 (an F-clade PP2C) or PP7 (a PPP-type phosphatase) did not prevent AHA2 from supporting growth on glucose media.

We also used the yeast system to establish an in vitro phosphatase assay to examine SAUR regulation of PP2C-D1 activity against AHA2. Plasma membrane fractions were prepared from RS-72 expressing AHA2. When recombinant PP2C-D1 was

added to these membrane fractions, Thr-947 was completely dephosphorylated within 10 min (Figure 4D). We therefore tested the ability of SAUR9, which displayed the strongest inhibitory activity in our pNPP assays, to inhibit PP2C-D1–mediated dephosphorylation of AHA2. Addition of a 3-fold molar excess of recombinant 6xHis-SAUR9 largely abolished PP2C-D1–mediated dephosphorylation of Thr-947. The slight reduction in phosphorylation that is apparent at 10 min is likely due to an endogenous phosphatase activity present in the membrane fractions, as this was also observed in mock reactions (Figure 4D, lane 3).

To obtain in planta support for the hypothesis that PP2C-D1 regulates PM H+-ATPase activity, we tested the possibility that PP2C-D1 and AHA2 can interact with one another in a bimolecular fluorescence complementation assay (Ohad et al., 2007). When cotransformed into *Nicotiana benthamiana* leaves, a strong plasma membrane–localized yellow fluorescent protein (YFP) signal was observed with AHA2 and PP2C-D1 split YFP constructs (Figure 4E). In contrast, neither AHA2 nor PP2C-D1 interacted with AUX1 split YFP constructs. Immunoblot analysis confirmed that the AUX1 split YFP constructs were indeed expressed in tobacco (Supplemental Figure 4). Thus, PP2C-D1 and PM H+-ATPases can interact at the plasma membrane in plants.

Genetic Analysis of PP2C-D Function

To examine potential roles for D-clade PP2Cs in plant growth and development, we analyzed T-DNA insertion alleles of eight of the nine *PP2C-D* genes. All eight single mutants exhibited no obvious defects in growth and development, suggesting functional redundancy. However, detailed inspection of these lines did reveal phenotypic similarities with SAUR19 overexpression seedlings, albeit weaker than GFP-SAUR19 controls. First, *pp2c-d5* seedlings exhibited a slight increase in hypocotyl length (Supplemental Figure 5). Due to likely functional redundancy, higher order *pp2c-d* mutant combinations may result in stronger phenotypes. Consistent with this notion, *pp2c-d1 pp2c-d2* double mutants displayed a long hypocotyl phenotype that was not apparent in either single mutant (Supplemental Figure 5). Second, like GFP-SAUR19 (Spartz et al., 2012), etiolated *pp2c-d1* seedlings exhibited reduced apical hook maintenance (Figure 5A), and introduction of the *pp2c-d2* mutation enhanced the apical hook defect of *pp2c-d1*. Although subtle, these phenotypes are consistent with PP2C-D phosphatases acting in an antagonistic manner to SAUR19.

To circumvent the likely functional redundancy of *PP2C-D* family members, we designed an artificial microRNA construct to target the *D2*, *D5*, *D7*, *D8*, and *D9* (amiD2/5/7/8/9) family

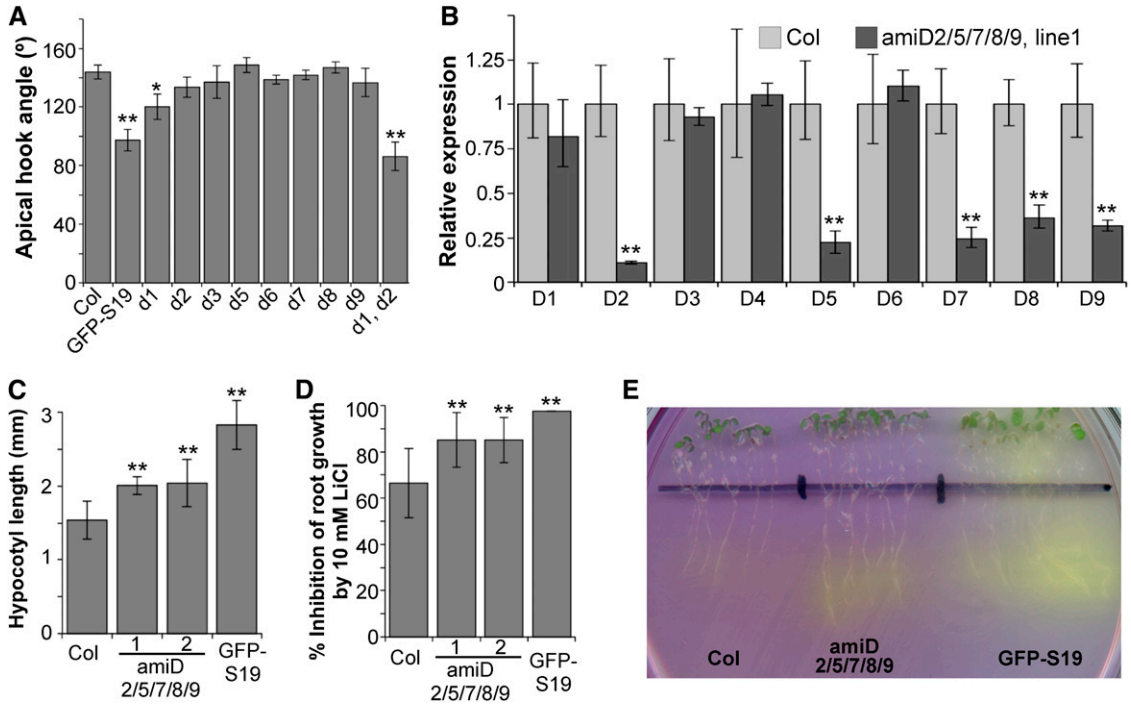

Figure 5. PP2C-D Family Loss-of-Function Studies.

(A) Quantification of apical hook angles of 5-d-old etiolated seedlings. Values indicate sample means ($n \geq 20$) ± SD.

(B) Quantitative RT-PCR assessing *PP2C-D* family gene expression in artificial micro RNA line. Values indicate sample means ± SD.

(C) Hypocotyl length of 8-d-old seedlings.

(D) Inhibition of root elongation by 10 mM LiCl. In **(C)** and **(D)**, values indicate sample means ± SD ($n \geq 15$).

(E) Media acidification around the root system of 9-d-old seedlings. Seedlings were grown for 7 d on ATS media and then transferred to plates containing bromocresol purple for 2 d. For all panels, asterisks indicate significant difference from Col control (one-way ANOVA; *$P < 0.05$; **$P < 0.01$).

members. Quantitative RT-PCR analysis of seedlings homozygous for this construct confirmed that the expression of all target genes was downregulated 3- to 10-fold, whereas nontargeted family members were largely unaffected (Figure 5B). Two independent lines expressing the amiD2/5/7/8/9 construct exhibited significant increases in hypocotyl length (Figure 5C). Furthermore, these lines also exhibited increases in LiCl sensitivity and media acidification (Figures 5D and 5E), suggesting that like SAUR19 gain-of-function plants, reductions in PP2C-D function result in elevated PM H^+-ATPase activity.

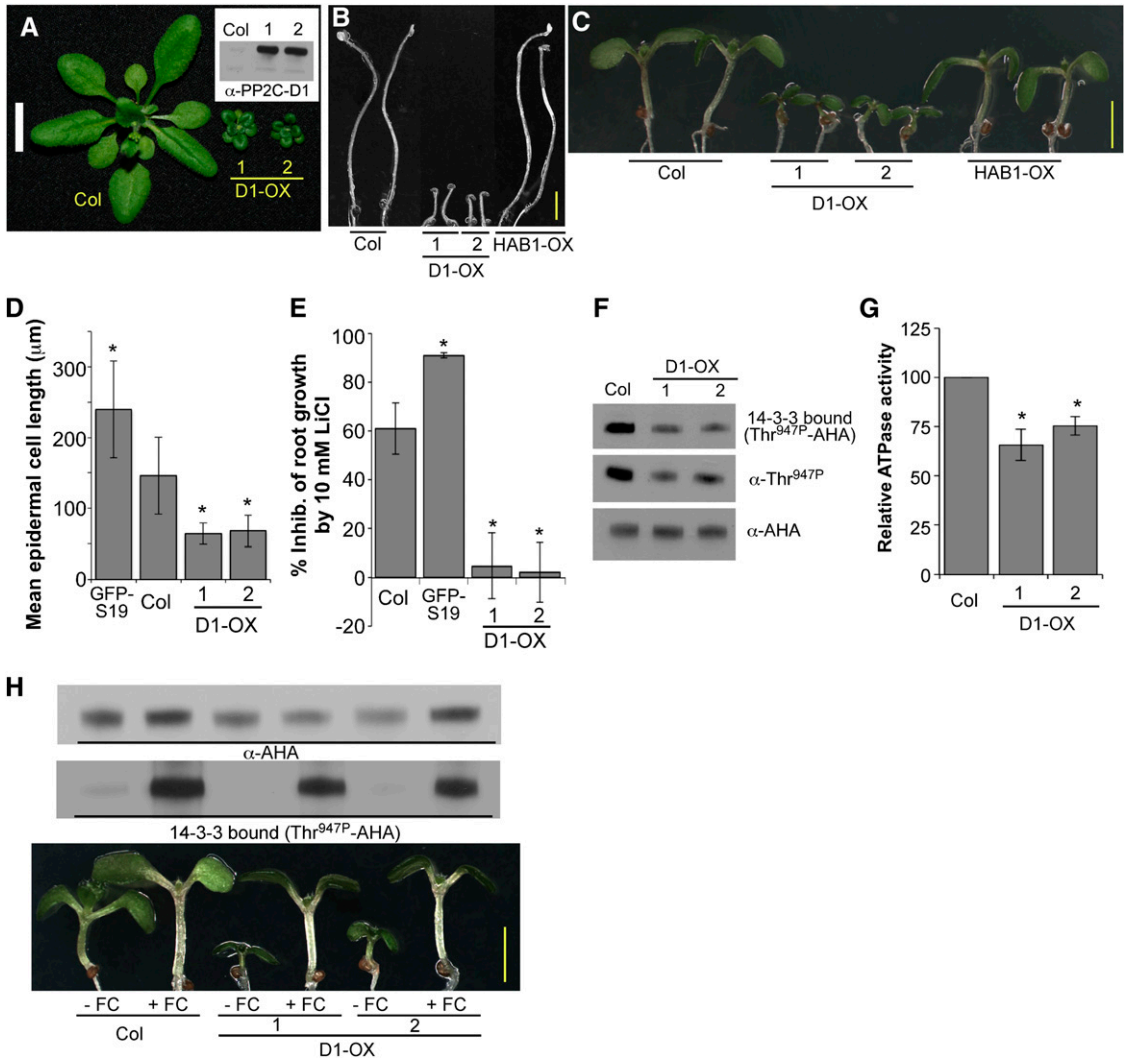

Figure 6. PP2C-D1 Negatively Regulates Cell Expansion.

(A) Twenty-five-day-old Col and *PP2C-D1* overexpression (D1-OX) plants. Two independent D1-OX lines are shown. Inset: α-PP2C-D immunoblot of the D1-OX lines depicted in **(A)**. Bar = 1 cm.

(B) and **(C)** *PP2C-D1* overexpression confers reduced hypocotyl length in both etiolated **(B)** and light-grown **(C)** 7-d-old seedlings. Bars = 2 mm.

(D) Mean epidermal cell length from 7-d-old light-grown seedling hypocotyls. The apical most 10 cells from 10 seedlings were measured. Error bars indicate SD.

(E) Inhibition of root elongation by 10 mM LiCl. Five-day-old seedlings were transferred to plates containing 10 mM LiCl and grown an additional 3 d. Values indicate sample means ± SD ($n \geq 20$).

(F) Examination of AHA C-terminal phosphorylation in 6-d-old etiolated seedlings by both GST-14-3-3 far-western gel blot and α-Thr^{947P} immunoblotting.

(G) Relative vanadate-sensitive ATP hydrolytic activity in plasma membrane fractions prepared from 6-d-old etiolated seedlings. Values represent the means ± SD obtained from three biological replicates.

(H) FC rescues the short hypocotyl phenotype of 35S:*PP2C-D1* plants. Bottom: Seedlings were grown for 4 d on ATS media and then transferred to media containing 1 μM FC for 3 d. Top: GST-14-3-3 far protein gel blot analysis of AHA C-terminal phosphorylation in Col and PP2C-D1 overexpression lines ± FC. For **(D)**, **(E)**, and **(G)**, asterisks indicate significant difference from Col as determined by one-way ANOVA; $P < 0.01$.

[See online article for color version of this figure.]

As an alternative genetic approach for probing PP2C-D function, we generated transgenic plants overexpressing *PP2C-D1* from the cauliflower mosaic virus 35S promoter. *PP2C-D1* overexpression conferred a dwarf phenotype, with striking reductions in leaf size and petiole length (Figure 6A). In seedlings, hypocotyl length was significantly diminished in both dark- and light-grown seedlings (Figures 6B and 6C). Unlike *PP2C-D1* overexpression, plants overexpressing the A-clade PP2C *HAB1* (Figures 6B and 6C; Saez et al., 2004) or the PPP-phosphatase *PP7* (Supplemental Figures 6A to 6C online; Liu et al., 2007; Sun et al., 2012) did not exhibit these reduced growth phenotypes. Reciprocally, whereas 35S:*HAB1* seedlings exhibited a strong ABA resistance phenotype, 35S:*PP2C-D1* seedlings displayed ABA sensitivity comparable to wild-type seedlings (Supplemental Figure 6D).

The reduction in hypocotyl length resulting from *PP2C-D1* overexpression was the result of diminished cell expansion, as hypocotyl epidermal cells were ~2.5-fold shorter than observed in wild-type Col control seedlings (Figure 6D). These reduced growth phenotypes conferred by *PP2C-D1* overexpression are in direct contrast to the increased growth phenotypes resulting from overexpression of stabilized SAUR19 derivatives (Spartz et al., 2012). Additionally, whereas GFP-SAUR19 root growth was hypersensitive to LiCl, seedlings overexpressing PP2C-D1 were highly resistant (Figure 6E).

Since we found that PP2C-D1 can negatively regulate AHA2 activity in yeast (Figure 4A), dephosphorylate AHA2 in vitro (Figure 4D), and interact with AHA2 in plants (Figure 4E), we examined PM H+-ATPase C-terminal phosphorylation status in seedlings overexpressing *PP2C-D1*. A clear reduction in Thr-947 phosphorylation was observed by both far-western gel blot and α-Thr^{947P} immunoblots of *PP2C-D1* overexpression extracts (Figure 6F). When assayed for vanadate-sensitive ATPase activity, plasma membrane fractions prepared from 35S:*PP2C-D1* seedlings exhibited approximately a 35% reduction in ATP hydrolytic activity compared with wild-type membranes (Figure 6G). Thus, as seen when heterologously expressed in yeast, PP2C-D1 can negatively regulate AHA function in plants.

If the growth defects conferred by PP2C-D1 overexpression are a direct consequence of reduced C-terminal phosphorylation of PM H+-ATPases, we reasoned that FC treatment might rescue these phenotypes. Indeed, 1 μM FC restored the hypocotyl length of 35S:PP2C-D1 seedlings to wild-type levels (Figure 6H, bottom). Furthermore, FC strongly promoted Thr-947 phosphorylation in PP2C-D1 overexpression seedlings (Figure 6H, top). This suggests that the reduction in PM H+-ATPase phosphorylation resulting from *PP2C-D1* overexpression is due to increased dephosphorylation activity as opposed to PP2C-D1 indirectly regulating Thr-947 phosphorylation by inhibiting the kinase(s) that phosphorylate this residue.

The above studies indicate that SAUR19 and PP2C-D proteins act in an antagonistic manner to regulate plant growth. To test this notion further, we introduced the 35S:*PP2C-D1* transgene into the GFP-SAUR19 background. *PP2C-D1* overexpression completely suppressed the long hypocotyl and LiCl hypersensitivity phenotypes of GFP-SAUR19 seedlings (Figures 7A and 7B). Furthermore, in 14-3-3 far-western gel blot assays, *PP2C-D1* overexpression suppressed the increased PM H+-ATPase C-terminal phosphorylation conferred by GFP-SAUR19 (Figure 7C). Suppression of these phenotypes occurred post-transcriptionally, as GFP-SAUR19 transcript levels were comparable to the GFP-SAUR19 parental line (Supplemental Figure 7). Thus, the finding that *PP2C-D1* overexpression can suppress SAUR19 overexpression phenotypes strongly supports the antagonistic relationship indicated by our enzymatic assays and genetic studies.

DISCUSSION

SAUR genes are present as large gene families in both higher and lower plants. While these genes have been used extensively as markers for auxin-inducible gene expression, their function in plant growth and development has remained elusive. However, recent genetic studies have implicated SAURs as positive effectors of cell expansion (Franklin et al., 2011; Chae et al., 2012; Spartz et al., 2012; Kong et al., 2013; Stamm and Kumar, 2013).

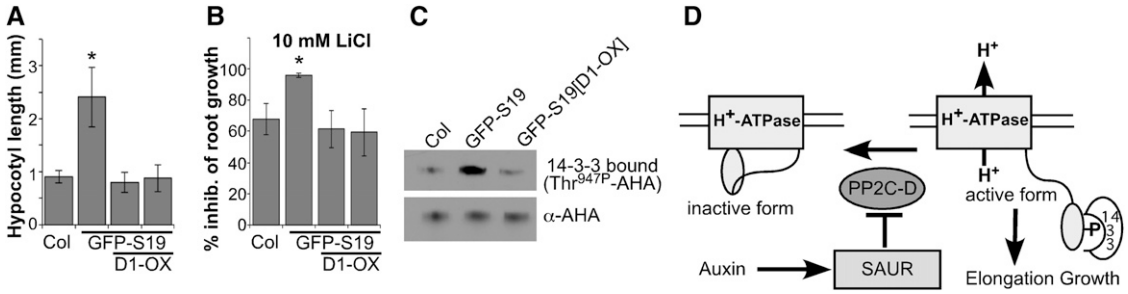

Figure 7. SAUR19 and PP2C-D1 Act Antagonistically.

(A) Hypocotyl lengths of 7-d-old seedlings. The GFP-SAUR19 parental line and two PP2C-D1 overexpression lines are shown. Values represent mean ($n \geq 18$) ± SD.

(B) Root growth assay on 10 mM LiCl. Values represent mean ($n \geq 12$) ± SD.

(C) GST-14-3-3 far-western gel blot analysis of AHA C-terminal phosphorylation.

(D) Model for SAUR regulation of PM H+-ATPases via repression of PP2C-D activity.

In **(A)** and **(B)**, asterisks indicate significant difference from Col controls as determined by one-way ANOVA; $P < 0.01$.

In this study, we describe a mechanism by which SAUR proteins promote cell expansion and plant growth. The genetic, molecular, and biochemical findings presented above suggest that SAUR proteins negatively regulate PP2C-D phosphatases to modulate PM H^+-ATPase activity (Figure 7D). In response to auxin, *SAUR* gene expression is rapidly induced, resulting in inhibition of PP2C-D phosphatases. This decrease in PP2C-D activity shifts PM H^+-ATPases toward the C-terminally phosphorylated, active state, which promotes cell expansion via an acid growth mechanism.

Auxin has long been implicated in PM H^+-ATPase activation (Cleland, 1976). However, the molecular components connecting auxin signaling to pump activation have remained elusive. Our findings demonstrate that SAUR proteins are intimately involved in this process, as the expression of stabilized SAUR fusion proteins phenocopies the constitutively active *ost2-2* mutant and results in increases in both the phosphorylation of a key regulatory phosphosite (Thr-947) and the enzymatic activity of PM H^+-ATPases. Furthermore, the loss-of-function *aha2-4* mutation significantly attenuates the phenotypes of StrepII-SAUR19 seedlings, demonstrating that SAUR19 overexpression phenotypes require PM H^+-ATPase activity.

Using an excised *Arabidopsis* hypocotyl system, Takahashi et al. (2012) recently demonstrated that auxin rapidly induces phosphorylation on Thr-947 of AHA proteins. This phosphorylation increase occurred within 10 min of IAA treatment and was not blocked by either anti-auxin treatment or mutation of the *TIR1* and *AFB2* auxin receptor genes, leading the authors to suggest that IAA promotes AHA phosphorylation independent of gene expression. A second study employing *Arabidopsis* suspension cells also detected increased phosphorylation of this residue up to 6 h after IAA treatment, suggesting that H^+-ATPase activation may persist for several hours (Chen et al., 2010). Previous physiological studies characterizing auxin-mediated growth of excised plant tissues have described a biphasic growth response: a rapid elongation phase occurring within minutes of auxin treatment, followed by a secondary elongation phase that clearly requires auxin-induced gene expression (Vanderhoef et al., 1976a, 1976b). The above model is only consistent with SAURs promoting this secondary response. However, one possibility is that SAUR activity as well as expression is regulated by auxin. If so, when coupled with the unstable nature of SAUR proteins, a biphasic growth response would result: rapid growth resulting from auxin activation of existing SAUR proteins, which are quickly degraded, followed by a secondary growth phase resulting from auxin-induced expression of *SAUR* genes. How auxin might regulate SAUR protein activity remains a topic for future study. However, the fact that auxin had no effect on SAUR19/PP2C-D1 interactions suggests that it does not bind directly. Given prior findings suggesting a role for AUXIN BINDING PROTEIN1 (ABP1) in promoting cell expansion (Jones et al., 1998) and H^+-ATPase activation (Barbier-Brygoo et al., 1989; Ruck et al., 1993), it is tempting to speculate that ABP1-mediated signaling may be involved. This possibility is particularly attractive give recent findings that ABP1 signaling is mediated by the TMK family of receptor-like kinases, as *tmk* mutants exhibit dramatic cell expansion defects (Dai et al., 2013; Xu et al., 2014). Alternatively, SAUR proteins may specifically mediate the delayed IAA-induced elongation response by sustaining H^+-ATPase activation via the attenuation of phosphatases that dephosphorylate and inactivate the H^+ pump. Our finding that SAUR proteins interact with and inhibit members of the PP2C-D clade of type 2C phosphatases is consistent with this possibility.

Our biochemical, genetic, and functional studies of *PP2C-D* genes strongly support the hypothesis that SAURs antagonize these phosphatases to modulate PM H^+-ATPase activity and promote plant growth. In addition to the inhibition of PP2C-D enzymatic activity observed in vitro, our genetic and biochemical studies reveal that SAUR19 and PP2C-D1 play opposing roles in regulating both cell expansion and H^+-ATPase activity. As is the case for *SAUR* genes, loss-of-function genetic studies of *PP2C-D* genes are significantly complicated by apparent functional redundancy within the nine-member *PP2C-D* family. That said, our analysis of plants expressing an artificial microRNA that partially knocks down the expression of five *PP2C-D* family members supports our model, as these plants exhibit increases in hypocotyl elongation, media acidification, and lithium hypersensitivity like GFP-SAUR19 plants. Furthermore, we demonstrate that PP2C-D1 can physically interact with AHA2 in planta and can negatively regulate PM H^+-ATPase activity both in planta and when heterologously expressed in yeast.

Determining precisely which subset of PP2C-D phosphatases interacts with which SAUR proteins to regulate specific processes is a future challenge. While SAUR19 (Spartz et al., 2012) and SAUR63 (Chae et al., 2012) family proteins are largely associated with the plasma membrane, other SAUR proteins have been reported to be cytosolic or nuclear localized (Knauss et al., 2003; Park et al., 2007; Kant et al., 2009; Kong et al., 2013). This suggests that these non-PM-associated SAUR proteins may not regulate H^+-ATPases similar to SAUR19. However, we speculate that different PP2C-D family members may localize to distinct cellular compartments, and colocalizing SAUR proteins may also regulate the activity of these phosphatases to modulate the activities of additional phosphoproteins.

Lastly, we note that in addition to auxin, the expression of many *SAUR* genes is induced by other growth-promoting pathways, including brassinosteroids, gibberellin, and the PIF transcription factors (Bai et al., 2012; Oh et al., 2012). This raises the intriguing possibility that SAUR-mediated activation of PM H^+-ATPases via the inhibition of PP2C-D activity may represent a regulatory module that is common to several growth promoting pathways.

METHODS

Plant Materials and Growth Conditions

All plants used in this study are in the Col-0 ecotype with the exception of 35S:*PP7-myc*, which is in the Wassilewskija ecotype. The *ost2-2* and *aha2-4* PM H^+-ATPase mutants and the 35S:*GFP-SAUR19* (line 1-1) and 35S:*StrepII-SAUR19* (line 2f) transgenic lines have been previously described (Merlot et al., 2007; Haruta et al., 2010; Spartz et al., 2012). Seedlings were grown at 20 to 22°C under 24 h fluorescent light (65 to 80 $\mu E\, m^{-2}\, s^{-1}$) on ATS media ± supplements as indicated. Adult plants were grown under long-day (16:8 h) lighting. *pp2c-d* T-DNA insertion mutants

were obtained from the ABRC: *pp2c-d1*/SALK_099356, *pp2c-d2*/WsDsLOX493G12, *pp2c-d3*/SALK_036920, *pp2c-d5*/GABI_330E08, *pp2c-d6*/SAIL_171H03, *pp2c-d7*/SALK_118712, *pp2c-d8*/SALK_143298, *pp2c d9*/SALK_026300C. The PP2C-D1 overexpression construct was generated by cloning the PCR-amplified genomic locus from Col plants into pEarleyGate100 (Earley et al., 2006) and subsequently introduced into Col and GFP-SAUR19 plants by *Agrobacterium tumefaciens*–mediated transformation. The estrogen-inducible GFP-SAUR19 binary vector was generated by Gateway cloning GFP-SAUR19 into pER8-GW. The StrepII-SAUR19 transgene was introduced into the *aha2-4* background by crossing.

For all root growth assays, seedlings were grown 4 to 5 d on ATS media (Lincoln et al., 1990) containing 10 g/L sucrose. Seedlings were then transferred to ATS plates containing various supplements, and the position of the root tips was marked. Seedlings were grown an additional 4 d and root growth measured. Percentage of inhibition was calculated based on the amount of root growth that occurred on unsupplemented ATS control plates. For media acidification assays, 8- to 12-d-old seedlings were transferred to water-agar plates containing 0.003% bromocresol purple and 30 μM Tris, pH 6.0. Color changes were documented 4 to 48 h after transfer. Apoplastic pH measurements were conducted using the infiltration/centrifugation method as previously described (Cho et al., 2012). Fluorescence of 8-hydroxypyrene-1,3,6-trisulfonic acid trisodium (Invitrogen) was determined with a Bio-Tek Synergy HT plate reader (excitation = 460 nm) and emission collected at 510 and 530 nm. Apical hook angles were measured from 5-d-old etiolated seedlings as previously described (Willige et al., 2012). All growth experiments were repeated a minimum of three times.

Statistical Analysis

Differences between control and experimental variants/treatments were analyzed by one-way ANOVA and significance assessed by Dunnett's test.

Yeast Two-Hybrid Screen

The SAUR19 coding sequence was cloned in-frame with the $GAL4^{DBD}$ of plasmid pBI880. The two-hybrid parent vectors, screening procedure, and *Arabidopsis thaliana* library have been previously described (Gray et al., 1999).

Yeast Complementation Assays

Saccharomyces cerevisiae strain RS-72 (*MATa, ade1-100, his4-519, leu2-3, 312, pPMA1:pGAL1*) and the *pPMA1:AHA2* expression plasmid pMP1745 have been previously described (Fuglsang et al., 2007). *PP2C-D1*, *PP2C-D5*, *PP7*, or *At1g43900* cDNAs containing *Not*I linkers were cloned into the *Not*I site of the pMP1612 expression vector (Fuglsang et al., 2007). These plasmids or the empty pRS315 or pMP1612 control vectors were introduced into RS-72 by LiAc transformation. Complementation of PMA1 activity was assessed by spotting serial dilutions of cultures grown in SG+His media onto SD+His (pH 6.5) plates, which were then incubated at 30°C for 4 d. The $D^{276}N$ mutation within the predicted metal binding domain of PP2C-D1 was introduced by QuikChange mutagenesis (Agilent Technologies).

Far-Western Gel Blot Assays

Plasma membrane fractions were prepared from 4- to 6-d-old seedlings by two-phase partitioning as previously described (Ito and Gray, 2006), with the exception that 10 mM NaF was included in all protein buffers. Two to five micrograms of plasma membrane proteins were mixed with SDS-PAGE sample buffer, separated by SDS-PAGE, and blotted to nitrocellulose. Far-western gel blot assays were performed as previously described (Hayashi et al., 2010) with the exception that an α-GST-HRP conjugate (GE Healthcare) was used to detect GST-14-3-3 (GF14ø) binding.

ATPase Assays

For ATPase measurements of yeast plasma membranes, RS-72 expressing AHA2 and PP2C-D1 or vector controls were grown to approximately 3×10^7 cells/mL in SG+His medium. Cultures were then diluted with 4 volumes of SD+His medium and grown for 4 h. Yeast plasma membranes were isolated by discontinuous density gradient centrifugation as previously described (Panaretou and Piper, 2006). Final membrane pellets were resuspended in 5 mM HEPES, 3 mM KCl, 0.1 mM EDTA, 330 mM sucrose, 1 mM DTT, and 1 mM PMSF, pH 7.8. Vanadate-sensitive ATPase activity was determined in enzymatically coupled assays by measuring the absorbance decrease of NADH at 340 nm (Regenberg et al., 1995). Two to three micrograms of plasma membranes were added to each reaction and absorbance readings taken every 5 min for a period of 20 min. Three biological replicates were performed.

For ATPase measurements from *Arabidopsis*, plasma membrane fractions were obtained by two-phase partitioning from 6-d-old etiolated seedlings grown in liquid ATS media. Vanadate-sensitive ATP hydrolytic activity was assessed in a coupled assay (Regenberg et al., 1995) with 0.05% Brij-58 included in the assay buffer (Johansson et al., 1995). One to two micrograms of plasma membranes were used per assay. Absorbance readings were taken every 2 min over a period of 14 min. Two technical replicates from each of three biological replicates were performed.

Antibodies

GFP monoclonal antibody was purchased from Covance. Polyclonal AHA and Thr^{947P} sera were generously provided by T. Kinoshita (Nagoya University) and have been previously described (Hayashi et al., 2010). To generate polyclonal antibodies against PP2C-D1, the PP2C-D1 coding sequence was cloned into the *Sal*I/*Not*I sites of pET28a (Novagen). The 6xHis-PP2C-D1 fusion protein was purified from BL21(DE3) cells using Ni-NTA agarose (Qiagen) in 6 M urea, 50 mM Tris, pH 7.5, 150 mM NaCl, 0.5% Nonidet P-40, 2 mM DTT, and 1 mM PMSF. The purified protein was subsequently dialyzed overnight in the same buffer with 2 M urea and then used for serum production by standard procedures (Cocalico Biologicals). For coimmunoprecipitation experiments, microsomal fractions prepared from 7-d-old light-grown GFP-SAUR19 or GFP-SAUR19[35S:PP2C-D1] seedlings were solubilized by dilution with 5 volumes PBS containing 1.5% Triton X-100 for 1 h at 4°C, followed by 1 h centrifugation at 20,000*g*. Four microliters of PP2C-D1 antisera or preimmune sera was incubated with 250 μg solubilized microsomes for 2 h at 4°C, and immune complexes captured with 25 μL Protein A agarose (Thermo). Immune complexes were washed three times with 1 mL PBS containing 1% Triton X-100. Following SDS-PAGE and transfer to nitrocellulose, GFP-SAUR19 and PP2C-D1 proteins were detected by immunoblotting with α-GFP and α-PP2C-D1 antibodies, respectively.

Protein Expression and Phosphatase Assays

GST-PP2C-D, GST-ABI1, At3g06270, and PP7 fusion constructs were made by Gateway recombination (Life Technologies) between pDEST15 (Life Technologies) and donor clones generated either by PCR (Supplemental Table 1) or available as cDNAs from the ABRC (D2: G83653, D3:G23137, D4:G67169, D8:G12341, and At3g06270:G23183). 6xHIS-tagged SAUR9, 19, 40, and 72 constructs were made by Gateway recombination into pET32-GW (N. Olszewski) from SAUR donor clones generated by PCR (Supplemental Table 1). Construction of GST-SAUR19 has been previously described (Spartz et al., 2012). *Escherichia coli* cultures expressing GST- or 6xHIS- tagged SAUR or PP2C proteins were

lysed by a French press in lysis buffer (50 mM Tris, pH 7.6, 100 mM NaCl, 2 mM $MnCl_2$, 10 mM $MgCl_2$, 1 mM EDTA, 1 mM DTT, and 0.25% Triton X-100) and purified with glutathione-agarose or Ni-NTA agarose beads. Free glutathione (15 mM) or 200 mM imidazole was used for elution. For phosphatase assays, 0.2 to 0.3 μM PP2C was preincubated with 0.2 to 1.6 μM SAUR proteins or an equivalent amount of elution buffer for 10 min. Protein mixtures were then added to assay buffer containing 75 mM Tris, pH 7.6, 10 mM $MnCl_2$, 100 mM NaCl, 0.5 mM EDTA, and 5 mM pNPP (unless otherwise indicated) to obtain a final volume of 100 μL. Absorbance at 405 nm was recorded every minute up to 20 min on a Powerwave 340 plate reader (Biotek Instruments). A standard curve was generated using 4-nitrophenol, and GraphPad Prism6 (GraphPad Software) statistical analysis software was used to perform nonlinear regression and to calculate V_{max} and K_m.

For AHA2 desphosphorylation assays, yeast plasma membranes were isolated from RS-72 cells expressing AHA2 as described above. Membranes were resuspended in 5 mM potassium phosphate, pH 7.8, 3 mM KCl, 0.1 mM EDTA, 330 mM sucrose, 1 mM DTT, 1 mM PMSF, solubilized with 0.1% Triton X-100, and diluted to 0.35 mg/mL. One microliter each of 25 mM $MnCl_2$ and purified MBP-PP2C-D1 fusion protein (50 ng/μL) in 25 mM Bis-Tris, pH 6.5, 0.3 M NaCl, 10 mM $MgCl_2$, and 2 mM $MnCl_2$ were added to 14-μL diluted plasma membranes, and reactions incubated at 25°C for 0 to 10 min. Where indicated, 6xHis-SAUR9 (or buffer control) was premixed with MBP-PP2C-D1 for 10 min on ice. Reactions were stopped with SDS-PAGE sample buffer, and AHA2 Thr-947 phosphorylation status was assessed by GST-14-3-3 far-western gel blotting as described above.

Quantitative RT-PCR

Primers utilized for assessing gene expression are listed in Supplemental Table 1. RNA was prepared from 7-d-old light-grown seedlings with the RNAeasy Plant Mini Kit (Qiagen) and included an on-column DNase treatment. Two micrograms of RNA was used for cDNA synthesis with M-MLV reverse transcriptase. Quantitative RT-PCR reactions were performed on the LightCycler System (Roche Applied Sciences) using SYBR Green JumpStart Taq ReadyMix (Sigma-Aldrich). Expression levels were normalized to *ACT7*, and three biological replicates were performed.

Bimolecular Fluorescence Complementation

Full-length coding sequences lacking stop codons of *AHA2*, *PP2C-D1*, and *AUX1* were amplified by PCR (Supplemental Table 1) and Gateway (Invitrogen) cloned into pENTR/D-TOPO or pDONR207. The cDNA inserts were subsequently recombined into the pSPYNE and pSPYCE (Walter et al., 2004) destination vectors using Gateway LR Clonase II Enzyme Mix (Invitrogen) to generate BiFC expression constructs. Binary vectors were introduced into *Agrobacterium* strain GV3101 (with the pMP90 helper plasmid) by electroporation. Bimolecular fluorescence complementation assays to visualize protein interactions were performed in a tobacco transient expression system (Schütze et al., 2009). Confocal microscopy was performed with a Nikon A1 spectral confocal microscope.

Artificial MicroRNA Construction

The artificial microRNA designer within the online WMD interface (Schwab et al., 2006; Ossowski et al., 2008) was used to design an artificial microRNA targeting *PP2CD2*, *D5*, *D7*, *D8*, and *D9* (see Supplemental Table 1 for primers). The D2/5/7/8/9 amiRNA was generated in the mi319a backbone of pRS300 (Ossowski et al., 2008) and subsequently introduced as a *Kpn*I-*Spe*I fragment behind the 35S promoter of pMDC44.

Accession Numbers

Arabidopsis Genome Initiative locus identifiers for the genes mentioned in this study are as follows: *SAUR19* (At5g18010), *SAUR9* (At4g36110), *SAUR40* (At1g79130), *SAUR72* (At3g12830), *ABI1* (At4g26080), *PP2C-D1* (At5g02760), *PP2C-D2* (At3g17090), *PP2C-D3* (At3g12620), *PP2C-D4* (At3g55050), *PP2C-D5* (At4g38520), *PP2C-D6* (At3g51370), *PP2C-D7* (At5g66080), *PP2C-D8* (At4g33920), *PP2C-D9* (At5g06750), *AHA1* (At2g18960), *AHA2* (At4g30190), *AUX1* (At2g38120), *PP7* (At5g63870), and *HAB1* (At1g72770).

Supplemental Data

The following materials are available in the online version of this article.

Supplemental Figure 1. Additional Phenotypes of SAUR19 Overexpression Plants.

Supplemental Figure 2. Characterization of PP2C-D Phosphatases.

Supplemental Figure 3. The $D^{276}N$ Mutation Abolishes Phosphatase Activity of PP2C-D1.

Supplemental Figure 4. Expression of AUX1 BiFC Constructs in Tobacco.

Supplemental Figure 5. Hypocotyl Lengths of 7-d-Old *pp2c-d* Mutants.

Supplemental Figure 6. Phosphatase Overexpression Controls.

Supplemental Figure 7. Quantitative RT-PCR Analysis of GFP-*SAUR19* and *PP2C-D1* Overexpression.

Supplemental Table 1. Primers Used in This Study

ACKNOWLEDGMENTS

We thank Miyoshi Haruta, Jeff Leung, Min Ni, Pedro Rodriguez, and the ABRC for providing seed stocks, Toshinori Kinoshita for providing α-AHA and α-Thr^{947P} antisera and the GST-14-3-3 expression construct, Anja Fuglsang for providing yeast strain RS-72 and expression vectors, and Neil Olszewski, John Ward, and Florence Gleason for numerous helpful discussions. We also thank John Ward for providing his plate reader for our phosphatase assays, the Jane Glazebrook lab for providing tobacco plants, and Joe Ecker for alerting us of the PP2C-D/SAUR interactions in the AI-1 database. This work was supported by grants from the National Science Foundation (MCB-0817205) and the National Institutes of Health (GM067203). S.H.L. was supported in part by Grant NRF-2012R1A1A2041366 from the National Research Foundation of Korea. M.R.S. received support from the U.S. Department of Energy Office of Basic Energy Sciences (DEFG02-88ER13938).

AUTHOR CONTRIBUTIONS

W.M.G., P.J.O., M.R.S., A.K.S., and H.R. designed the research. W.M.G., A.K.S., H.R., M.Y.P., K.N.G., S.H.L., and A.S.M. performed the research and analyzed data. W.M.G., A.K.S., and H.R. wrote the article.

Received April 3, 2014; revised April 3, 2014; accepted May 5, 2014; published May 23, 2014.

REFERENCES

Arabidopsis Interactome Mapping Consortium (2011). Evidence for network evolution in an Arabidopsis interactome map. Science **333:** 601–607.

Bai, M.Y., Shang, J.X., Oh, E., Fan, M., Bai, Y., Zentella, R., Sun, T.P., and Wang, Z.Y. (2012). Brassinosteroid, gibberellin and

phytochrome impinge on a common transcription module in Arabidopsis. Nat. Cell Biol. **14:** 810–817.

Barbier-Brygoo, H., Ephritikhine, G., Klämbt, D., Ghislain, M., and Guern, J. (1989). Functional evidence for an auxin receptor at the plasmalemma of tobacco mesophyll protoplasts. Proc. Natl. Acad. Sci. USA **86:** 891–895.

Baxter, I., Tchieu, J., Sussman, M.R., Boutry, M., Palmgren, M.G., Gribskov, M., Harper, J.F., and Axelsen, K.B. (2003). Genomic comparison of P-type ATPase ion pumps in Arabidopsis and rice. Plant Physiol. **132:** 618–628.

Chae, K., Isaacs, C.G., Reeves, P.H., Maloney, G.S., Muday, G.K., Nagpal, P., and Reed, J.W. (2012). Arabidopsis SMALL AUXIN UP RNA63 promotes hypocotyl and stamen filament elongation. Plant J. **71:** 684–697.

Chapman, E.J., and Estelle, M. (2009). Mechanism of auxin-regulated gene expression in plants. Annu. Rev. Genet. **43:** 265–285.

Chen, Y., Hoehenwarter, W., and Weckwerth, W. (2010). Comparative analysis of phytohormone-responsive phosphoproteins in *Arabidopsis thaliana* using TiO2-phosphopeptide enrichment and mass accuracy precursor alignment. Plant J. **63:** 1–17.

Cho, D., Villiers, F., Kroniewicz, L., Lee, S., Seo, Y.J., Hirschi, K.D., Leonhardt, N., and Kwak, J.M. (2012). Vacuolar CAX1 and CAX3 influence auxin transport in guard cells via regulation of apoplastic pH. Plant Physiol. **160:** 1293–1302.

Cleland, R.E. (1976). Fusicoccin-induced growth and hydrogen ion excretion of Avena coleoptiles: Relation to auxin responses. Planta **128:** 201–206.

Cohen, P. (1989). The structure and regulation of protein phosphatases. Annu. Rev. Biochem. **58:** 453–508.

Dai, N., Wang, W., Patterson, S.E., and Bleecker, A.B. (2013). The TMK subfamily of receptor-like kinases in Arabidopsis display an essential role in growth and a reduced sensitivity to auxin. PLoS ONE **8:** e60990.

Das, A.K., Helps, N.R., Cohen, P.T., and Barford, D. (1996). Crystal structure of the protein serine/threonine phosphatase 2C at 2.0 A resolution. EMBO J. **15:** 6798–6809.

Earley, K.W., Haag, J.R., Pontes, O., Opper, K., Juehne, T., Song, K., and Pikaard, C.S. (2006). Gateway-compatible vectors for plant functional genomics and proteomics. Plant J. **45:** 616–629.

Franklin, K.A., Lee, S.H., Patel, D., Kumar, S.V., Spartz, A.K., Gu, C., Ye, S., Yu, P., Breen, G., Cohen, J.D., Wigge, P.A., and Gray, W.M. (2011). Phytochrome-interacting factor 4 (PIF4) regulates auxin biosynthesis at high temperature. Proc. Natl. Acad. Sci. USA **108:** 20231–20235.

Frías, I., Caldeira, M.T., Pérez-Castiñeira, J.R., Navarro-Aviñó, J.P., Culiañez-Maciá, F.A., Kuppinger, O., Stransky, H., Pagés, M., Hager, A., and Serrano, R. (1996). A major isoform of the maize plasma membrane H(+)-ATPase: characterization and induction by auxin in coleoptiles. Plant Cell **8:** 1533–1544.

Fuglsang, A.T., Guo, Y., Cuin, T.A., Qiu, Q., Song, C., Kristiansen, K.A., Bych, K., Schulz, A., Shabala, S., Schumaker, K.S., Palmgren, M.G., and Zhu, J.K. (2007). Arabidopsis protein kinase PKS5 inhibits the plasma membrane H+-ATPase by preventing interaction with 14-3-3 protein. Plant Cell **19:** 1617–1634.

Fuglsang, A.T., Visconti, S., Drumm, K., Jahn, T., Stensballe, A., Mattei, B., Jensen, O.N., Aducci, P., and Palmgren, M.G. (1999). Binding of 14-3-3 protein to the plasma membrane H(+)-ATPase AHA2 involves the three C-terminal residues Tyr(946)-Thr-Val and requires phosphorylation of Thr(947). J. Biol. Chem. **274:** 36774–36780.

Gray, W.M., del Pozo, J.C., Walker, L., Hobbie, L., Risseeuw, E., Banks, T., Crosby, W.L., Yang, M., Ma, H., and Estelle, M. (1999). Identification of an SCF ubiquitin-ligase complex required for auxin response in *Arabidopsis thaliana*. Genes Dev. **13:** 1678–1691.

Gévaudant, F., Duby, G., von Stedingk, E., Zhao, R., Morsomme, P., and Boutry, M. (2007). Expression of a constitutively activated plasma membrane H+-ATPase alters plant development and increases salt tolerance. Plant Physiol. **144:** 1763–1776.

Hagen, G., and Guilfoyle, T. (2002). Auxin-responsive gene expression: genes, promoters and regulatory factors. Plant Mol. Biol. **49:** 373–385.

Hager, A. (2003). Role of the plasma membrane H+-ATPase in auxin-induced elongation growth: historical and new aspects. J. Plant Res. **116:** 483–505.

Haruta, M., and Sussman, M.R. (2012). The effect of a genetically reduced plasma membrane protonmotive force on vegetative growth of Arabidopsis. Plant Physiol. **158:** 1158–1171.

Haruta, M., Burch, H.L., Nelson, R.B., Barrett-Wilt, G., Kline, K.G., Mohsin, S.B., Young, J.C., Otegui, M.S., and Sussman, M.R. (2010). Molecular characterization of mutant Arabidopsis plants with reduced plasma membrane proton pump activity. J. Biol. Chem. **285:** 17918–17929.

Hayashi, Y., Nakamura, S., Takemiya, A., Takahashi, Y., Shimazaki, K., and Kinoshita, T. (2010). Biochemical characterization of in vitro phosphorylation and dephosphorylation of the plasma membrane H+-ATPase. Plant Cell Physiol. **51:** 1186–1196.

Hayashi, Y., Takahashi, K., Inoue, S., and Kinoshita, T. (2014). Abscisic acid suppresses hypocotyl elongation by dephosphorylating plasma membrane H+-ATPase in *Arabidopsis thaliana*. Plant Cell Physiol. **55:** 845–853.

Ito, H., and Gray, W.M. (2006). A gain-of-function mutation in the Arabidopsis pleiotropic drug resistance transporter PDR9 confers resistance to auxinic herbicides. Plant Physiol. **142:** 63–74.

Jelich-Ottmann, C., Weiler, E.W., and Oecking, C. (2001). Binding of regulatory 14-3-3 proteins to the C terminus of the plant plasma membrane H+-ATPpase involves part of its autoinhibitory region. J. Biol. Chem. **276:** 39852–39857.

Johansson, F., Olbe, M., Sommarin, M., and Larsson, C. (1995). Brij 58, a polyoxyethylene acyl ether, creates membrane vesicles of uniform sidedness. A new tool to obtain inside-out (cytoplasmic side-out) plasma membrane vesicles. Plant J. **7:** 165–173.

Jones, A.M., Im, K.H., Savka, M.A., Wu, M.J., DeWitt, N.G., Shillito, R., and Binns, A.N. (1998). Auxin-dependent cell expansion mediated by overexpressed auxin-binding protein 1. Science **282:** 1114–1117.

Kant, S., Bi, Y.M., Zhu, T., and Rothstein, S.J. (2009). SAUR39, a small auxin-up RNA gene, acts as a negative regulator of auxin synthesis and transport in rice. Plant Physiol. **151:** 691–701.

Kinoshita, T., and Shimazaki, Ki. (1999). Blue light activates the plasma membrane H(+)-ATPase by phosphorylation of the C-terminus in stomatal guard cells. EMBO J. **18:** 5548–5558.

Kinoshita, T., and Shimazaki, K. (2001). Analysis of the phosphorylation level in guard-cell plasma membrane H+-ATPase in response to fusicoccin. Plant Cell Physiol. **42:** 424–432.

Knauss, S., Rohrmeier, T., and Lehle, L. (2003). The auxin-induced maize gene ZmSAUR2 encodes a short-lived nuclear protein expressed in elongating tissues. J. Biol. Chem. **278:** 23936–23943.

Kong, Y., Zhu, Y., Gao, C., She, W., Lin, W., Chen, Y., Han, N., Bian, H., Zhu, M., and Wang, J. (2013). Tissue-specific expression of SMALL AUXIN UP RNA41 differentially regulates cell expansion and root meristem patterning in Arabidopsis. Plant Cell Physiol. **54:** 609–621.

Lincoln, C., Britton, J.H., and Estelle, M. (1990). Growth and development of the axr1 mutants of Arabidopsis. Plant Cell **2:** 1071–1080.

Liu, H.T., Li, G.L., Chang, H., Sun, D.Y., Zhou, R.G., and Li, B. (2007). Calmodulin-binding protein phosphatase PP7 is involved in thermotolerance in Arabidopsis. Plant Cell Environ. **30:** 156–164.

Ma, Y., Szostkiewicz, I., Korte, A., Moes, D., Yang, Y., Christmann, A., and Grill, E. (2009). Regulators of PP2C phosphatase activity function as abscisic acid sensors. Science **324:** 1064–1068.

Marre, E. (1979). Fusicoccin: A tool in plant physiology. Annu. Rev. Plant Physiol. **30:** 273–288.

Merlot, S., Leonhardt, N., Fenzi, F., Valon, C., Costa, M., Piette, L., Vavasseur, A., Genty, B., Boivin, K., Müller, A., Giraudat, J., and Leung, J. (2007). Constitutive activation of a plasma membrane H (+)-ATPase prevents abscisic acid-mediated stomatal closure. EMBO J. **26:** 3216–3226.

Nemhauser, J.L., Hong, F., and Chory, J. (2006). Different plant hormones regulate similar processes through largely nonoverlapping transcriptional responses. Cell **126:** 467–475.

Oh, E., Zhu, J.Y., and Wang, Z.Y. (2012). Interaction between BZR1 and PIF4 integrates brassinosteroid and environmental responses. Nat. Cell Biol. **14:** 802–809.

Ohad, N., Shichrur, K., and Yalovsky, S. (2007). The analysis of protein-protein interactions in plants by bimolecular fluorescence complementation. Plant Physiol. **145:** 1090–1099.

Ossowski, S., Schwab, R., and Weigel, D. (2008). Gene silencing in plants using artificial microRNAs and other small RNAs. Plant J. **53:** 674–690.

Paciorek, T., Zazímalová, E., Ruthardt, N., Petrásek, J., Stierhof, Y.D., Kleine-Vehn, J., Morris, D.A., Emans, N., Jürgens, G., Geldner, N., and Friml, J. (2005). Auxin inhibits endocytosis and promotes its own efflux from cells. Nature **435:** 1251–1256.

Panaretou, B., and Piper, P. (2006). Isolation of yeast plasma membranes. Methods Mol. Biol. **313:** 27–32.

Park, J.E., Kim, Y.S., Yoon, H.K., and Park, C.M. (2007). Functional characterization of a small auxin-up RNA gene in apical hook development in Arabidopsis. Plant Sci. **172:** 150–157.

Park, S.Y., et al. (2009). Abscisic acid inhibits type 2C protein phosphatases via the PYR/PYL family of START proteins. Science **324:** 1068–1071.

Rayle, D.L., and Cleland, R. (1970). Enhancement of wall loosening and elongation by Acid solutions. Plant Physiol. **46:** 250–253.

Rayle, D.L., and Cleland, R.E. (1980). Evidence that auxin-induced growth of soybean hypocotyls involves proton excretion. Plant Physiol. **66:** 433–437.

Rayle, D.L., and Cleland, R.E. (1992). The Acid Growth Theory of auxin-induced cell elongation is alive and well. Plant Physiol. **99:** 1271–1274.

Regenberg, B., Villalba, J.M., Lanfermeijer, F.C., and Palmgren, M.G. (1995). C-terminal deletion analysis of plant plasma membrane H(+)-ATPase: yeast as a model system for solute transport across the plant plasma membrane. Plant Cell **7:** 1655–1666.

Robert, S., et al. (2010). ABP1 mediates auxin inhibition of clathrin-dependent endocytosis in Arabidopsis. Cell **143:** 111–121.

Ruck, A., Palme, K., Venis, M.A., Napier, R.M., and Felle, H.H. (1993). Patch-clamp analysis establishes a role for an auxin binding protein in the auxin stimulation of plasma membrane current in *Zea mays* protoplasts. Plant J. **4:** 41–46.

Saez, A., Apostolova, N., Gonzalez-Guzman, M., Gonzalez-Garcia, M.P., Nicolas, C., Lorenzo, O., and Rodriguez, P.L. (2004). Gain-of-function and loss-of-function phenotypes of the protein phosphatase 2C HAB1 reveal its role as a negative regulator of abscisic acid signalling. Plant J. **37:** 354–369.

Schwab, R., Ossowski, S., Riester, M., Warthmann, N., and Weigel, D. (2006). Highly specific gene silencing by artificial microRNAs in Arabidopsis. Plant Cell **18:** 1121–1133.

Schweighofer, A., Hirt, H., and Meskiene, I. (2004). Plant PP2C phosphatases: emerging functions in stress signaling. Trends Plant Sci. **9:** 236–243.

Schütze, K., Harter, K., and Chaban, C. (2009). Bimolecular fluorescence complementation (BiFC) to study protein-protein interactions in living plant cells. Methods Mol. Biol. **479:** 189–202.

Singh, J., and Roberts, M.R. (2004). Fusicoccin activates pathogen-responsive gene expression independently of common resistance signalling pathways, but increases disease symptoms in *Pseudomonas syringae*-infected tomato plants. Planta **219:** 261–269.

Spartz, A.K., Lee, S.H., Wenger, J.P., Gonzalez, N., Itoh, H., Inzé, D., Peer, W.A., Murphy, A.S., Overvoorde, P.J., and Gray, W.M. (2012). The SAUR19 subfamily of SMALL AUXIN UP RNA genes promote cell expansion. Plant J. **70:** 978–990.

Stamm, P., and Kumar, P.P. (2013). Auxin and gibberellin responsive Arabidopsis SMALL AUXIN UP RNA36 regulates hypocotyl elongation in the light. Plant Cell Rep. **32:** 759–769.

Sun, X., Kang, X., and Ni, M. (2012). Hypersensitive to red and blue 1 and its modification by protein phosphatase 7 are implicated in the control of Arabidopsis stomatal aperture. PLoS Genet. **8:** e1002674.

Takahashi, K., Hayashi, K., and Kinoshita, T. (2012). Auxin activates the plasma membrane H^+-ATPase by phosphorylation during hypocotyl elongation in Arabidopsis. Plant Physiol. **159:** 632–641.

Vanderhoef, L.N., Stahl, C.A., and Lu, T.Y. (1976a). Two elongation responses to auxin respond differently to protein synthesis inhibition. Plant Physiol. **58:** 402–404.

Vanderhoef, L.N., Stahl, C.A., Williams, C.A., and Brinkmann, K.A. (1976b). Additional evidence for separable responses to auxin in soybean hypocotyl. Plant Physiol. **57:** 817–819.

Walter, M., Chaban, C., Schütze, K., Batistic, O., Weckermann, K., Näke, C., Blazevic, D., Grefen, C., Schumacher, K., Oecking, C., Harter, K., and Kudla, J. (2004). Visualization of protein interactions in living plant cells using bimolecular fluorescence complementation. Plant J. **40:** 428–438.

Willige, B.C., Ogiso-Tanaka, E., Zourelidou, M., and Schwechheimer, C. (2012). WAG2 represses apical hook opening downstream from gibberellin and PHYTOCHROME INTERACTING FACTOR 5. Development **139:** 4020–4028.

Xu, T., et al. (2014). Cell surface ABP1-TMK auxin-sensing complex activates ROP GTPase signaling. Science **343:** 1025–1028.